Raman-active modes in homogeneous and inhomogeneous bundles of single-walled carbon nanotubes

2009 J. Phys.: Condens. Matter 21 045302

(http://iopscience.iop.org/0953-8984/21/4/045302)

J. Phys.: Condens. Matter **21** (2009) 045302 (7pp) doi:10.1088/0953-8984/21/4/045302

Raman-active modes in homogeneous and inhomogeneous bundles of single-walled carbon nanotubes

K Sbai[1], A Rahmani[1,3], H Chadli[1] and J-L Sauvajol[2]

[1] Laboratoire de Physique des matériaux et Modélisation des Systèmes, Université Moulay Ismaïl, Faculté des Sciences, BP 11201, Zitoune, 50000 Meknès, Morocco
[2] Laboratoire des Colloïdes, Verres et Nanomatériaux (UMR CNRS 5587), Université Montpellier II, F-34095 Montpellier Cedex 5, France

E-mail: rahmani@fs-umi.ac.ma

Received 4 July 2008, in final form 24 November 2008
Published 19 December 2008
Online at stacks.iop.org/JPhysCM/21/045302

Abstract

In the present work, the non-resonant Raman-active modes are calculated for several diameters, chiralities and sizes for homogeneous and inhomogeneous bundles of single-walled carbon nanotubes (BWCNTs), using the spectral moment's method (SMM). Additional intense Raman-active modes are present in the breathing-like modes (BLM) spectra of these systems in comparison with a single fully symmetric A_{1g} mode characteristic of isolated nanotubes (SWCNTs). The dependence of the wavenumber of these modes in terms of diameters, lengths and number of tubes was investigated. We found that, for a finite (in)homogeneous bundle, additional breathing-like modes appear as a specific signature.

(Some figures in this article are in colour only in the electronic version)

1. Introduction

Since the discovery of carbon nanotubes in 1991 [1], the attention of both experimentalists and theoreticians has focused on their properties. In particular, single-walled carbon nanotubes have currently been intensively investigated worldwide for their intrinsic one-dimensional properties and their promising applications. Among the techniques extensively used to characterize these materials, Raman scattering plays a preponderant role [2].

The Raman spectrum of SWCNT is dominated below 500 cm^{-1} by the radial breathing modes (RBM) and in the high wavenumber region, between 1400 and 1600 cm^{-1}, by the tangential modes (TM). The assignment of the band below 500 cm^{-1} was carried out using the results of force constants of the lattice dynamics of isolated nanotubes [3, 4], tight-binding [5–7] and *ab initio* [8–10] calculations for the zone-center phonons, and a bond-polarizability model [4] for the Raman intensity. Raman studies have shown that the radial breathing mode in the low wavenumber region shows a straightforward dependence on the diameter of the SWCNT that can be used to determine the distribution of tube diameters [4, 11]. The TM shape depends strongly on whether the tube is metallic or semiconducting [12–14]. In the intermediate wavenumber range, 600–1400 cm^{-1}, the intensity of the Raman spectrum is weak and several peaks were observed. After a period of controversy [15–18], substantial progress was made in the interpretation of the Raman activity in this range by considering both the nanotube electronic structure and a double resonance process [19–21].

Isolated single-wall carbon nanotubes can be grown on a Si/SiO_2 substrate containing catalytic iron nanoparticles [22], using a CVD method [23]. In production methods of bundled SWCNTs [24], the direct comparison between theory and experiment is difficult because of the wide range of diameters and chiralities usually present in the samples. The resonance Raman intensity for a defined nanotube has a strong diameter and chirality dependence. By changing the laser excitation energies, one can determine the population of specific nanotubes in the sample [21]. The analysis of Raman data recorded using theoretical models based on infinite tubes has been frequently applied as a tool to analyze the SWCNT mean diameter and diameter distribution in both bulk and nanoscopic samples. The exact strength of the

[3] Author to whom any correspondence should be addressed.

intertube interaction within a bundle was the subject of several studies [2, 6, 9, 25–27]. From these studies, this intertube interaction induced an upshift of the RBM of about 8–16 cm^{-1} which is determined by the competition between the intertube and intratube interactions. A second mode with predominant breathing-like character is also reported in the BM region [25, 27]. However, one has to be aware that the finite length and number of tubes forming a bundle as well as inhomogeneity effects have to be included in the detailed analysis.

In a previous paper [28], by using the spectral moment's method (SMM) in the framework of the bond-polarization theory, we have calculated the polarized Raman spectra of chiral and achiral SWCNTs as a function of their diameter and length. An investigation of finite-size effects was extended to large finite lengths up to 85 nm as well as to achiral and chiral tubes of several diameters. The dependence of tangential modes on chirality and the dependence of the Raman spectrum on the tube length was clearly observed.

In this work, we study the Raman spectra of single-wall carbon nanotube bundles in the framework of polarizability theory. Their dependence on the diameters, lengths, chiralities and the number of (identical or different) tubes in the bundle is investigated. It is obvious that the Raman intensity calculated by this non-resonant method cannot match the experimental spectra, which display a strong resonant character in carbon nanotubes. Nevertheless, the SMM predictions concerning the number and frequencies of Raman-active lines as a function of diameter, length and chirality do not depend on the resonant process of Raman scattering. As a consequence, the SMM predictions can help to interpret the frequencies of the Raman-active modes.

2. Models and method

Let us recall that the ideal nanotube structure can be obtained from a graphene sheet by rolling it up along the straight line connecting two lattice points into a seamless cylinder in such a way that the two points coincide [4]. Following the usual terminology of [3], the tube can be specified by integers (n, m) that define the translation vector between the two points. Alternatively, the tube can be described by its diameter D and the chiral angle θ, which is the angle between the tube circumference and the nearest zigzag of carbon–carbon bonds. The tube is called achiral for $\theta = 0°$ (zigzag type) and $\theta = 30°$ (armchair type), and chiral for $0° < \theta < 30°$. The diameter D of a single-wall carbon nanotube is given by

$$D = a\sqrt{3m^2 + nm + n^2}/\pi, \tag{1}$$

with $a = 1.42$ Å.

When SWCNTs are closely packed together, a three-dimensional carbon bundle is formed. From the diffraction profile of the crystalline ropes of SWCNTs, it has been previously reported that these systems can be represented by two-dimensional infinite trigonal lattices of uniform cylinders [29]. For a finite-size bundle, the nanotubes were placed parallel to one another on a finite-size trigonal array of cell parameter $a_0 = D + d_{t-t}$, where d_{t-t} represents the intertube spacing. The intertube interaction energy is minimized with respect to the intertube separation and the angle of simultaneous rotation of all tubes about their axes. The optimized intertube separations, d_{t-t}, are roughly equal to 0.32 nm. This value, slightly smaller than the inter-graphene sheets' distance in graphite, is in agreement with calculations [25, 30] and experiments [31]. The number of tubes per bundle is called N_t.

In the present work, we calculate the polarized Raman spectra for finite and infinite bundles. The C–C intratube interactions are described by using the same force constant set as used in our calculations of the Raman spectra of isolated SWCNTs [28] and formally introduced by Saito [11]. A Lennard-Jones potential:

$$U_{LJ} = 4\epsilon[(\sigma/R)^{12} - (\sigma/R)^6], \tag{2}$$

is used to describe the van der Waals intertube interactions between the tubes in a bundle, with parameters $\epsilon = 2.964$ meV and $\sigma = 0.3407$ nm [28, 32]. These values have recently been found to describe correctly the van der Waals contribution to the C_{60} bulk cohesive energy [33, 34].

In the SWCNTs' Raman study, we use the non-resonant bond-polarizability model [35] to describe the coupling between vibrational modes and photons. By the way SWCNTs bundle, we neglect the van der Waals intertube interaction effects on the bond-polarizability model parameters.

A usual method to calculate the Raman spectrum requires, besides the polarization parameters, the eigenvalues and the eigenvectors which can be obtained by direct diagonalization of the dynamical matrix of the system. However, when the system contains a large number of atoms, as for long finite SWCNT bundles, the dynamical matrix is very large and its diagonalization fails or requires long computing time. In contrast, the spectral moment's method allows us to compute directly the Raman spectrum of very large harmonic systems without any diagonalization of the dynamical matrix [28, 36, 37]. Otherwise, for small samples, both approaches lead exactly to the same position and intensity for the different peaks. The spectral moment's method consists of developing the resolvent $R(z)$ of the response of the system, $J(u)$, which can be written as $(z = u + i\epsilon)$ [36]

$$J(u) = -\frac{1}{\pi} \lim_{\epsilon \to 0_+} \mathrm{Im}[R(z)], \tag{3}$$

in a continued fraction:

$$R(z) = \cfrac{b_0}{z - a_1 - \cfrac{b_1}{z - a_2 - \cfrac{b_2}{z - a_3 - \cfrac{b_3}{\ddots}}}}, \tag{4}$$

where the coefficients a_n and b_n are given by

$$a_{n+1} = \frac{\bar{\nu_n}}{\nu_n}; \qquad b_n = \frac{\nu_n}{\nu_{n-1}}. \tag{5}$$

The spectral generalized moments ν_n and $\bar{\nu_n}$ of $J(u)$ are directly obtained from the dynamical matrix $\tilde{D}$. As shown in our earlier works [28, 36, 37], a sharp truncation of the

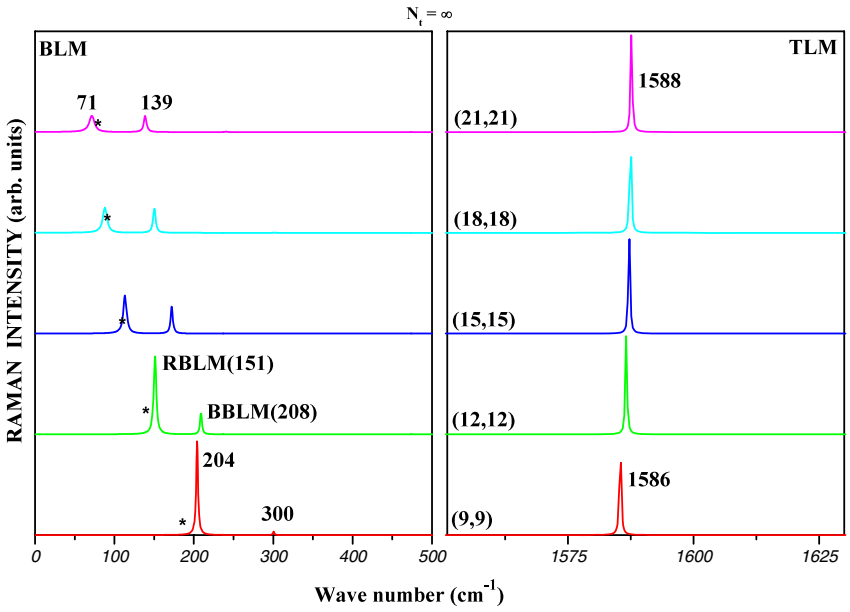

Figure 1. The ZZ calculated Raman spectra of (n, n) SWCNT crystals for $n = 9$, 12, 15, 18 and 21 from bottom to top. The stars give the position of the RBM of isolated tubes.

continued fraction leads to the appearance of sharp lines in the calculated low-frequency spectrum. On the other hand, the calculations of Raman and infrared spectra show that a limited number of moments are sufficient to obtain the frequency of active modes with a good accuracy. In this work 500 moments have been used.

3. Results and discussion

Using the spectral moment's method, the Raman-active-mode wavenumbers are directly obtained from the position of the peaks in the calculated Raman spectra. The lineshape of each peak is assumed to be Lorentzian and the linewidth is fixed at 1.7 cm^{-1}. The intensity of the Raman spectrum is normalized with respect to the number of carbon atoms in the sample under consideration. In all our calculations, the nanotube axis is along the Z axis and a carbon atom is along the X axis of the nanotube reference frame. The laser beam is kept along the y axis of the reference frame. We consider that both incident and scattered polarizations are along the z axis to calculate the polarized ZZ spectra. More than 50 000 atoms in carbon nanotubes were treated.

3.1. Infinite homogeneous bundles of identical infinite SWCNTs (BWCNTs)

Firstly, the calculations are performed on infinitely homogeneous bundles (crystal: $N_t = \infty$) of SWCNTs of several diameters. We recall that infinite SWCNTs are obtained by applying periodic conditions on unit cells of the studied nanotubes. The results for typical armchair tubes (9, 9), (12, 12), (15, 15), (18, 18) and (21, 21) are reported in figure 1, where the ZZ Raman spectra are displayed in the low wavenumber or breathing-like mode (BLM: on the left) region and in the high wavenumber or tangential-like mode (TLM: on the right) region.

In the TLM region, all spectra display the peaks corresponding to A_{1g} modes. Shifts for A_{1g} modes are observed when the tube diameter increases. In the BLM region, the ZZ spectra exhibit two peaks denoted here as RBLM (for radial breathing-like mode) and BBLM (for bundle breathing-like mode). The RBLM and BBLM modes arise from radial breathing and doubly degenerate (E symmetry) modes in SWCNTs. These two modes (denoted BM(1) and BM(2) in [25, 27]) are full symmetric modes with breathing-like shapes (figure 5 in [25]). The comparison between the Raman spectra of the SWCNTs and BWCNTs shows the appearance of a second mode (BBLM) at a wavenumber higher than that of the RBLM one. For all modes, we observe a downshift with increasing tube diameter. One can see that, for small nanotube diameters, only the RBLM has an important intensity and this mode is associated with a nearly pure breathing-like eigenvector. For a diameter larger than 1.4 nm, the intertube interactions affect the RBLM mode patterns and the eigenvector of this mode shows a clear hexagonal deformation. As a consequence, the upshift of RBLM becomes less important in comparison with relatively rigid tube modes. For $D > 2.0$ nm, the RBLM mode has a wavenumber lower than the RBM wavenumber of SWCNTs. At the same time, the intertube interactions largely dominate over the intratube ones and the higher wavenumber mode BBLM becomes more and more intense. The frequency and the vibration pattern of these modes are determined by the competitions between the intertube and intratube interactions. In [25, 27], beside the prediction of a second mode of breathing character (BM(2)), the authors show that the frequency of BM(1) has an upward shift of 15 cm^{-1} for small diameter, diminishes to zero for a diameter close to 2 nm and has a downward shift for larger diameter. These results are well reproduced in this SMM study.

To illustrate the BLM wavenumber dependence on nanotube diameter, we have reported in figure 2, on a log–log

Table 1. A/D^{α} law for SWCNT and BWCNT wavenumber modes: $A(\mathrm{cm}^{-1}\ \mathrm{nm})$.

	E^{s}_{1g}	E^{s}_{2g}	A^{s}_{1g}	E^{b}_{1g}	E^{b}_{2g}	RBLM $D < D_c$	RBLM $D > D_c$	BBLM $D < D_c$	BBLM $D > D_c$
A	158.5	496.9	224.4	163.8	490.8	244.9	285.0	380.6	308.2
α	1.00	1.00	1.00	0.78	0.92	0.98	1.31	1.23	0.79

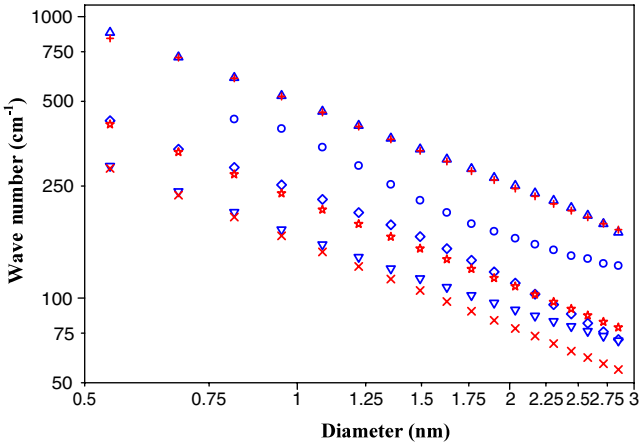

Figure 2. Diameter dependence, in log–log scale, of the Raman-active modes wavenumbers for SWCNT crystals: $E^{s}_{1g}(\times)$, A^{s}_{1g} (★) and $E^{s}_{2g}(+)$ for SWCNTs and $E^{b}_{1g}(\triangledown)$, RBLM (◊), $E^{b}_{2g}(\triangle)$ and BBLM (○) for BWCNTs.

scale, the wavenumber of $E^{s}_{1g}(\times)$, $A^{s}_{1g}(\bigstar)$ and $E^{s}_{2g}(+)$ modes for isolated SWCNTs and $E^{b}_{1g}(\triangledown)$, RBLM (◊), $E^{b}_{2g}(\triangle)$ and BBLM (○) for bundles of SWCNTs versus nanotube diameter D. From table 1 and for isolated SWCNTs, we show that the wavenumber modes obey the A/D^{α} law, with α close to 1 and $A = 158.5$, 496.9 and 224.4 cm^{-1} nm for E^{s}_{1g}, E^{s}_{2g} and A^{s}_{1g} modes, respectively. The latter value is close to the values obtained by other works. One can observe that this linear relationship between inverse tube diameter and the RBM mode wavenumbers stated for isolated nanotubes was affected by the presence of neighboring tubes. The evolution of the BWCNT wavenumber modes E^{b}_{1g} and E^{b}_{2g} is characterized by coefficients A and α different from those found in the case of SWCNTs: $A = 163.8$ and 490.8 cm^{-1} nm with $\alpha = 0.78$ and 0.92 for E^{b}_{1g} and E^{b}_{2g}, respectively. The variation of wavenumber of RBLM and BBLM according to the diameter of the tube seems characterized by two sets of parameters: when $D < D_c$, we obtain values of $A = 244.9$ and 380.6 cm^{-1} nm with $\alpha = 0.98$ and 1.23, whereas, when $D > D_c$, these values are close to $A = 380.6$ and 308.2 cm^{-1} nm with $\alpha = 1.23$ and 0.79 for RBLM and BBLM modes, respectively. The calculated D_c value is 1.75 ± 0.25 nm. This value is close to that obtained by Henrard *et al* [25] within a valence force field (VFF) model. For small diameters, the tubes are relatively rigid and with the increase of the diameter they soften so as to become flexible for larger diameters. As a consequence, the field of intertube forces is governed by two regimes with a crossover D_c which can be related to the deformation of the tube surface. With regard to the Raman intensity, we observe a decrease of the intensity with the increase in the diameter except for the BBLM modes. If we consider the variation of the Raman intensity ratio $I_{\mathrm{BBLM}}/I_{\mathrm{RBLM}}$, we observe a growth of this ratio, when the diameter of the tube increases to reach a value of 1 for a diameter close to D_c.

3.2. Finite homogeneous BWCNTs

To study the effects of finite size on homogeneous BWCNT Raman-active modes, we developed calculations of the Raman spectra of bundles of different numbers of infinite nanotubes. As mentioned above, in finite-size bundles, the nanotubes were placed parallel to each other on a finite-size trigonal array to form concentric shells.

In figure 3, we report the ZZ polarized Raman spectra for a typical (9, 9) armchair BWCNTs for four numbers of tubes $N_t = 1$, 7, 19 and 91 in comparison with the crystal system. Firstly, we observe that the TLM region is slightly affected by the increase of N_t. From $N_t = 1$ to crystal, the wavenumber of the A_{1g} mode passes from 1585 to 1586 cm^{-1}. Concerning the BLM region, the ZZ spectrum shows, besides the A_{1g} shift from 183 cm^{-1} for SWCNTs to 204 cm^{-1} for infinite BWCNTs, additional peaks around the A_{1g} wavenumber mode for given finite values of N_t. For example, for $N_t = 19$, two additional peaks are observed at wavenumbers 195 and 209 cm^{-1}. The more the size of the beam increases, the more the additional peaks around A_{1g} are grouped together to form the single peak around 204 cm^{-1} for an infinite beam. These behaviors have a simple explanation by considering the tubes in the bundle as coupled oscillators. Indeed, the interactions between identical oscillators lead to vibrational modes of strongly mixed character. In some cases the BLMs are not uniform radial motions; rather they are strongly mixed with totally symmetric components of doubly degenerate tube modes which split into finite BWCNTs due to the low symmetry of the system. We note the presence of the BBLM around the wavenumber 300 cm^{-1} for all values of $N_t > 1$. In comparing our calculations that are in agreement with Henrard's *et al* VVF model work [25] for the dimer (9, 9) (9, 9), we observe two peaks located around 206 and 187 cm^{-1} assigned to in-phase and out-of-phase breathing modes, respectively. As predicted by the authors, and depending on the tube diameter, we show that the bundle constituted by larger numbers of tubes (19 for example) is still characterized by modes with mixed character around the out-of-phase one.

3.3. Inhomogeneous finite bundles of infinite SWCNTs

In section 3.2, we have studied the vibrational structure of bundles of identical tubes. But the present production

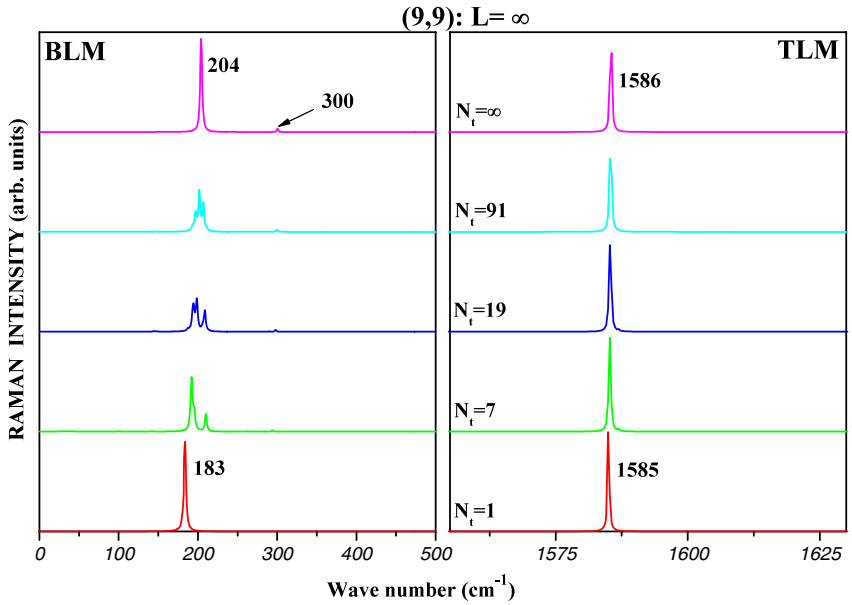

Figure 3. The calculated ZZ Raman spectra of finite-size (9, 9) BWCNTs as a function of the number of tubes in the bundle: $N_t = 1$, 7, 19, 91 and crystal from bottom to top.

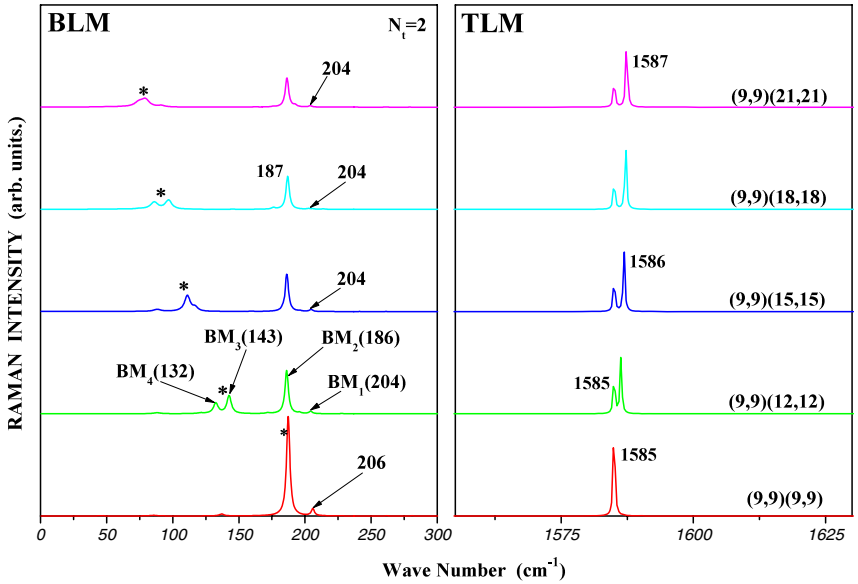

Figure 4. The ZZ calculated Raman spectra of inhomogeneous finite bundles of SWCNTs, formed with two SWCNTs of different diameters: (9, 9) (n, n), for $n = 9$, 12, 15, 18 and 21 (from the bottom to top), in BLM (on the left) and TLM (on the right) regions. The stars indicate the position of the RBM mode of isolated tubes.

techniques could lead to the formation of bundles constituted by tubes not necessarily with the same diameter or chirality. In this section we are interested in the effect of inhomogeneous finite bundles of SWCNTs, formed with infinite tubes of different diameters and chiralities. To define the positions of the two-tube (in)homogeneous bundle, if $\vec{x}$, $\vec{y}$ and $\vec{z}$ are basis vectors of the first SWCNT reference frame, the position of the second tube is given by the translation vector $\vec{T} = [(D_1 + D_2)/2 + d_{t-t}]\vec{y}$, where D_1, D_2 and d_{t-t} represent the diameter of tubes and the intertube spacing, respectively.

Firstly, the calculations are performed on finite bundles of identical infinitely long ($L = \infty$) SWCNTs of several diameters. The results of a typical armchair system, formed with two infinite tubes with different diameters, denoted here as (9, 9) (n, n), are reported in figure 4 where the ZZ Raman spectra are displayed in the BLM (on the left) and TLM (on the right) regions. The behavior of the modes in the TLM region is the same as in the homogeneous system with two A_{1g} modes around 1585 cm^{-1} corresponding to the (9, 9) and (n, n) SWCNTs. In the BLM region, the ZZ spectra exhibit additional peaks denoted here as BM_n in comparison with the homogeneous system. From figure 4, we can conclude that the lower wavenumber pair of the peaks (modes BM_3 and BM_4) can be mainly related to a vibration of larger tubes and that

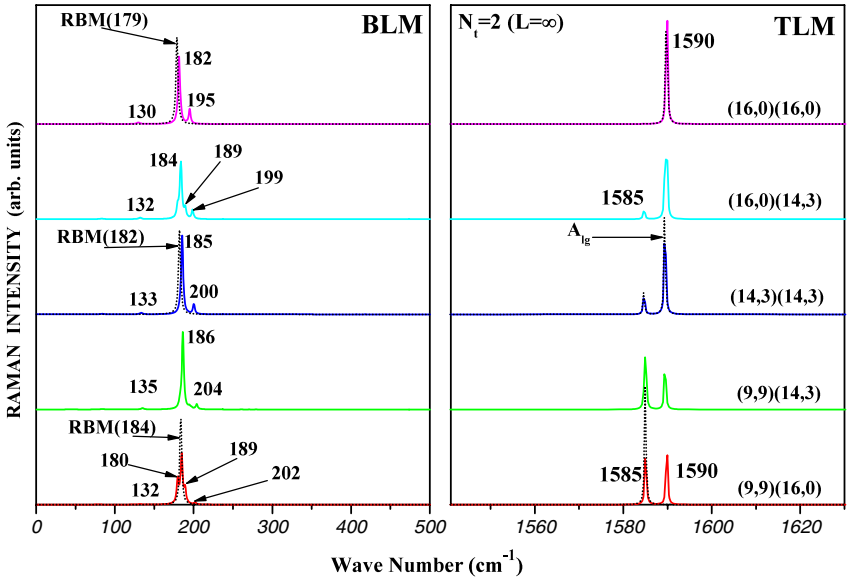

Figure 5. The ZZ calculated Raman spectra of inhomogeneous finite BWCNTs, formed with two SWCNTs of different chiralities: (9, 9) (n, m), in BLM (on the left) and TLM (on the right) ranges. Dashed lines indicate the ZZ calculated Raman spectra of corresponding SWCNTs.

higher wavenumber peaks can be associated to a vibration of the (9, 9) tube. We noted here that the mode BM_1 (around 204 cm^{-1}) found in a (9, 9) homogeneous bundle is observed in all case. Due to the lower symmetry of the environment, one can observe a splitting of the RBM mode of the larger tube into two components (down and upshifts) in particular for (12, 12) and (18, 18) tubes. This demonstrates that in such cases the experimental spectra would allow us to identify the individual components of the bundle even if the modes are split.

Secondly, in order to show the chirality of SWCNT effects on the bundle, we reported in figure 5 the results of Raman spectra of inhomogeneous finite bundles of SWCNTs, formed with two infinite tubes, approximately of the same diameters and different chiralities: (9, 9), (14, 3) and (16, 0), whose diameters are 1.237 nm, 1.247 nm and 1.27 nm, respectively. In the TLM region, the observed modes are close to those found in the homogeneous system with two A_{1g} active modes around 1585 and 1590 cm^{-1} corresponding to the (9, 9) and (n, m) SWCNTs, respectively. In the BLM region, the ZZ spectra exhibit additional peaks in comparison with the homogeneous system. Particularly for (9, 9) (16, 0), we observe a strong splitting of the RBM modes into several modes (downshifts and upshifts).

One can see that the calculated Raman spectrum of an inhomogeneous bundle of SWCNTs is not the sum of the individual tubes' spectra. The analysis of the chirality and the diameter inhomogeneity effects could be used to discriminate experimentally between homogeneous and inhomogeneous bundles. In particular, the observed splitting in TLM and BLM regions can be used as a specific signature of inhomogeneous bundles in the interpretation of experimental data. To achieve a satisfactory correspondence between theoretical and experimental work each individual bundle (with nonuniform diameter and/or chirality) has to be analyzed as a specific case and more information about the tubes (for example, their number) in the probed bundles should be given.

4. Conclusion

We have investigated Raman spectra of homogeneous and inhomogeneous bundles of SWCNTs. The analysis of results in the light of diameter and chirality dependence performed on SWCNT samples shows a real appropriateness with our model. The obtained results for homogeneous infinite bundles are consistent with previous works [25, 27]. Thanks to the spectral moment's method, we have investigated bundles consisting of more than 100 SWCNTs of several sizes. Finite-size (length and number of tubes) and inhomogeneity (chirality and diameters) effects are observed essentially in the BLM regions with additional/split modes which can be considered in the analysis of experimental data.

Acknowledgments

The work was supported by the Morocco–Spain Inter Academic Mixed Committee and a CNRS-France/CNRST-Morocco agreement.

References

[1] Iijima S 1991 *Nature* **354** 56
[2] Dresselhaus M S and Eklund P C 2000 *Adv. Phys.* **49** 705
[3] Dresselhaus M S, Dresslhaus G and Eklund P C 1996 *Science of Fullerenes and Carbon Nanotubes* (New York: Academic)
[4] Saito R, Takeya T, Kimura T, Dresselhaus G and Dresselhaus M S 1999 *Phys. Rev.* B **59** 2388

[5] Henrard L, Hernández E, Bernier P and Rubio A 1999 *Phys. Rev.* B **60** R8521
[6] Kahn D and Lu J P 1999 *Phys. Rev.* B **60** 6535
[7] Yu J, Kalia R K and Vashishta P 1995 *J. Chem. Phys.* **103** 6697
[8] Kürti J, Kresse G and Kuzmany H 1998 *Phys. Rev.* B **58** R8869
[9] Sánchez-Portal D, Artacho E, Soler J M, Rubio A and Ordejón P 1999 *Phys. Rev.* B **59** 12678
[10] Milneral M, Kürti J, Hulman M and Kuzmany H 2000 *Phys. Rev.* B **84** 1324
[11] Saito R, Takeya T, Kimura T, Dresselhaus G and Dresselhaus M S 1998 *Phys. Rev.* B **57** 4145
[12] Kataura H, Kumazawa Y, Maniwa Y, Umezu I, Suzuki S, Ohtsuka Y and Achiba Y 1999 *Synth. Met.* **103** 2555
[13] Alvarez L, Righi A, Guillard T, Rols S, Anglaret E, Laplaze D and Sauvajol J-L 2000 *Chem. Phys. Lett.* **316** 186
[14] Pimenta M A, Marucci A, Empedocles S A, Bawendi M G, Hanlon E B, Rao A M, Eklund P C, Smalley R E, Dresslhaus G and Dresslhaus M S 1998 *Phys. Rev.* B **58** R16016
[15] Rao A M, Richter E, Bandow S, Chase B, Eklund P C, Williams K A, Fang S, Subbaswamy K R, Menon M, Thess A, Smalley R E, Dresselhaus G and Dresselhaus M S 1997 *Science* **275** 187
[16] Anglaret E, Rols S and Sauvajol J-L 1998 *Phys. Rev. Lett.* **81** 4780
[17] Lamy de la Chapelle M, Lefrant S, Journet C, Maser W-K, Bernier P and Loiseau A 1998 *Carbon* **36** 705–8
[18] Lamy de la Chapelle M 1998 *Doctorat Thesis* Nantes University, France (October)
[19] Jorio A, Pimenta M A, Souza Filho A G, Saito R, Dresselhaus G and Dresselhaus M S 2003 *New J. Phys.* **5** 139.1
[20] Saito R, Grüneis A, Samsonidze Ge G, Brar V W, Dresselhaus G, Dresselhaus M S, Jorio A, Cançado L G, Fantini C, Pimenta M A and Souza Filho A G 2003 *New J. Phys.* **5** 157.1
[21] Saito R, Fantini C and Jiang J 2008 *Carbon Nanotubes* (*Springer Topics in Applied Physics* vol 111) (Berlin: Springer) p 251
[22] Hafner J H, Cheung C L, Oosterkamp T H and Lieber C M 2001 *J. Phys. Chem.* B **105** 743
[23] Jorio A, Saito R, Hafner J H, Lieber C M, Hunter M, McClure T, Dresselhaus G and Dresselhaus M S 2001 *Phys. Rev. Lett.* **86** 1118
[24] Dresselhaus M S, Dresselhaus G and Avouris Ph 2001 *Topics in Applied Physics* vol 80 (Berlin: Springer)
[25] Henrard L, Popov V N and Rubio A 2001 *Phys. Rev.* B **64** 205403
[26] Venkateswaran U D, Rao A M, Richter E, Menon M, Rinzler A, Smally R E and Eklund P C 1999 *Phys. Rev.* B **59** 10928
[27] Popov V N and Henrard L 2001 *Phys. Rev.* B **63** 233407
[28] Rahmani A, Sauvajol J-L, Rols S and Benoit C 2002 *Phys. Rev.* B **66** 125404
[29] Rols S, Almairac R, Henrard L, Anglaret E and Sauvajol J-L 1999 *Eur. Phys. J.* B **10** 263
[30] Charlier J C, Goze X and Michenaud J P 1995 *Europhys. Lett.* **29** 43
[31] Thess A, Jee R, Nikolaev P, Dai H, Petit P, Robert J, Xu C, Hee Lee Y, Gon Kim S, Rinzler A G, Colbert D T, Scuseria G E, Tomanek D, Fisher J E and Smalley R E 1996 *Science* **273** 483
[32] Rahmani A, Sauvajol J-L, Cambedouzou J and Benoit C 2005 *Phys. Rev.* B **71** 125402
[33] Ulbricht H, Moos G and Hertel T 2003 *Phys. Rev. Lett.* **90** 095501
[34] Chadli H, Rahmani A, Sbai K, Hermet P, Rols S and Sauvajol J-L 2006 *Phys. Rev.* B **74** 205412
[35] Guha S, Menendez J, Page J B and Adams G B 1996 *Phys. Rev.* B **53** 13106
[36] Benoit C, Royer E and Poussigue G 1992 *J. Phys.: Condens. Matter* **4** 3125
[37] Rahmani A, Jund P, Benoit C and Jullien R 2001 *J. Phys.: Condens. Matter* **13** 5413